EDGE ARTICLE

Check for updates

Unprecedented selectivity for homologous lectin targets: differential targeting of the viral receptors L-SIGN and DC-SIGN†

Clara Delaunay,‡[a] Sara Pollastri, ‡[b] Michel Thépaut,[a] Gianluca Cavazzoli,[b] Laura Belvisi, [b] Clémentine Bouchikri,[a] Nuria Labiod,[c] Fatima Lasala,[c] Ana Gimeno,[d] Antonio Franconetti, [d] Jesús Jiménez-Barbero, [def] Ana Ardá,[de] Rafael Delgado,[cg] Anna Bernardi *[b] and Franck Fieschi *[ah]

DC-SIGN (CD209) and L-SIGN (CD209L) are two C-type lectin receptors (CLRs) that facilitate SARS-CoV-2 infections as viral co-receptors. SARS-CoV-2 manipulates both DC-SIGN and L-SIGN for enhanced infection, leading to interest in developing receptor antagonists. Despite their structural similarity (82% sequence identity), they function differently. DC-SIGN, found in dendritic cells, shapes the immune response by recognizing pathogen-associated carbohydrate patterns. In contrast, L-SIGN, expressed in airway epithelial endothelial cells, is not directly involved in immunity. COVID-19's primary threat is the hyperactivation of the immune system, potentially reinforced if DC-SIGN engages with exogenous ligands. Therefore, L-SIGN, co-localized with ACE2-expressing cells in the respiratory tract, is a more suitable target for anti-adhesion therapy. However, designing a selective ligand for L-SIGN is challenging due to the high sequence identity of the Carbohydrate Recognition Domains (CRDs) of the two lectins. We here present **Man84**, a mannose ring modified with a methylene guanidine triazole at position 2. It binds L-SIGN with a K_D of 12.7μM ± 1 μM (ITC) and is the first known L-SIGN selective ligand, showing 50-fold selectivity over DC-SIGN (SPR). The X-ray structure of the L-SIGN CRD/**Man84** complex reveals the guanidinium group's role in achieving steric and electrostatic complementarity with L-SIGN. This allows us to trace the source of selectivity to a single amino acid difference between the two CRDs. NMR analysis confirms the binding mode in solution, highlighting **Man84**'s conformational selection upon complex formation. Dimeric versions of **Man84** achieve additional selectivity and avidity in the low nanomolar range. These compounds selectively inhibit L-SIGN dependent trans-infection by SARS-CoV-2 and Ebola virus. **Man84** and its dimeric constructs display the best affinity and avidity reported to date for low-valency glycomimetics targeting CLRs. They are promising tools for competing with SARS-CoV-2 anchoring in the respiratory tract and have potential for other medical applications.

Introduction

To detect pathogens and thus potential danger, antigen presenting cells of our immune system possess a battery of receptors, called pathogen recognition receptors (PRRs), that are dedicated to their surveillance and identification.[1] Among PRRs, C-type lectin receptors (CLRs) are dedicated to the recognition of carbohydrate molecular patterns associated with pathogens, and can then contribute to shape an immune response. This family of receptors shares a common domain, known as the Carbohydrate Recognition Domain (CRD), containing a conserved calcium binding site used for the recognition of carbohydrates. The diverse CLRs differ in size, oligomerization state and signaling pathways, and will therefore have a different impact on the

[a]Université Grenoble Alpes, CNRS, CEA, Institut de Biologie Structurale, Grenoble, France. E-mail: franck.fieschi@ibs.fr

[b]Università degli Studi di Milano, Dipartimento di Chimica, via Golgi 19, Milano, Italy. E-mail: anna.bernardi@unimi.it

[c]Instituto de Investigacion Hospital Universitario 12 de Octubre, Universidad Complutense, School of Medicine, Madrid, Spain

[d]Chemical Glycobiology Lab, Center for Cooperative Research in Biosciences (CIC bioGUNE), Basque Research and Technology Alliance (BRTA), 48160 Derio, Bizkaia, Spain

[e]Ikerbasque, Basque Foundation for Science, Bilbao, Spain

[f]Centro de Investigacion Biomedica En Red de Enfermedades Respiratorias, 28029 Madrid, Spain

[g]School of Medicine, Universidad Complutense, Madrid, Spain

[h]Institut Universitaire de France (IUF), Paris, France

immune system depending on the panels of glycans they recognize.[2,3] However, not all CLRs are strictly dedicated to immunity and some of them are even expressed in other cell types and tissues such as hepatocytes or endothelial cells from blood capillaries to airway epithelia.[4,5] These lectin receptors, therefore, have other functions such as physiological clearance mechanisms (e.g. asialoglycoprotein receptors[6]) and cell adhesion molecules (e.g. selectins[7]), for example.

Some pathogens have found strategies to bypass the role of CLRs in immunity activation and even hijack CLRs for their own benefit during the infection process. Thus, subversion of CLRs has been reported to turn these lectins into alternate receptors or attachment factors, notably by HIV,[8] Ebola virus[9] and SARS-CoV virus,[10,11] responsible for the severe acute respiratory syndrome (SARS) in 2002. In the context of the 2020 world-scale coronavirus outbreak, we,[12] and others,[13–15] tested the potential role of several CLRs toward the viral transmission process and found that only two of them, DC-SIGN and L-SIGN (CD209 and CD209L, respectively), are exploited by SARS-CoV-2 to enhance its infection. SARS-CoV-2 can interact with both lectins through its highly glycosylated Spike protein and uses them as anchor points at the cell surface. There is still a debate on the detail of this process: some groups have suggested DC/L-SIGN involvement as direct alternative receptors,[13,15] others only as promoters of a trans-infection mode, whereby the two CLRs play the role of attachment factors, enabling binding and concentration of viruses onto cell surfaces, before transferring it to its fusion receptor ACE2 on permissive cells along the respiratory tract.[12,14]

DC-SIGN and L-SIGN (also called DC-SIGNR for DC-SIGN Related) have a very high sequence similarity (82% for the whole protein,[16] and up to 72% for the sole Carbohydrate Recognition Domain). Both are tetrameric proteins and bind to mannosylated oligosaccharides.[17] The tetramers have similar, but not identical, topology and dynamics and this impacts on some aspects of their recognition profile of multivalent glycoconjugates.[18,19] Finally, a major difference between the two lectins is their expression in different cell types and tissues. DC-SIGN is expressed on immature dendritic cells, L-SIGN is expressed in human liver sinusoidal endothelial cells, human lung in type II alveolar cells and in endothelial cells and is co-expressed with ACE2 on respiratory tract cells.[15,20–22]

Because of its known role in various infections, DC-SIGN has already been the focus of intense efforts as a target for drug design, mostly employing glycomimetic ligands.[23–29] Glycomimetics are structural and/or functional mimics of carbohydrates used to replace the template molecules, typically as the ligand of a protein target.[30–32] We and others have developed monovalent and multivalent glycomimetic ligands of DC-SIGN and have used them as antagonists to block DC-SIGN-mediated infections of HIV, dengue fever and Ebola.[23–29] In a recent work, we demonstrated that using previously developed polyvalent glycomimetics we were able to block the trans-infection of SARS-CoV-2 mediated by DC-SIGN.[12] This suggested that antagonist glycomimetics could be efficient additions in the tool-box against SARS-CoV-2 spreading.

Despite the fact that L-SIGN is known to be the preferential attachment factor for West Nile Virus,[33] there was no report of antagonist development or simply of L-SIGN targeting in anti-infective strategy before the recent COVID 19 outbreak and the identification of L-SIGN as a potential target together with DC-SIGN. COVID 19 has been associated with hyperactivation of the immune system as a major threat for patients.[22] DC-SIGN is a dendritic cell PRR and it is not yet known whether its engagement by recognition of exogenous ligands could reinforce this hyperactivation. In contrast, L-SIGN is not involved in the mucosal immune response and colocalizes with ACE2-expressing cells in the lungs. Thus, in the case of SARS-CoV-2, for both reasons above, L-SIGN appears as a more relevant target than DC-SIGN for host-targeted antiviral therapies. We have recently reported a set of C2 triazole-modified mono- and pseudo-di-mannosides that inhibit both DC-SIGN and L-SIGN binding to SARS-CoV-2 spike, up to the low micromolar level.[34] However, all these molecules have more or less the same impact on the two receptors, or are slightly DC-SIGN selective. No selective ligand has yet been described for L-SIGN. This is not too surprising, considering the 72% identity of the two CRDs,[35] nonetheless, an L-SIGN selective ligand would be welcomed, both as a probe of the CLR' role in viral infections and for development as secure anti-adhesive antiviral. To further pursue this goal, we moved from the aminotriazole derivative 1 (**Man79**), which in our previous study[34] displayed an IC_{50} value $278 \pm 7 \mu M$ for L-SIGN and $318 \pm 2 \mu M$ for DC-SIGN (SPR experiment, binding inhibition to immobilized Spike). The binding mode of this molecule in DC-SIGN can be inferred from recently reported X-ray structures that show the existence of an ammonium binding site in the vicinity of the canonical Ca^{2+} ion.[24,29] This area is conserved in L-SIGN, which can explain the good affinity of 1 for this target. Comparison of the two lectins CRDs suggests that the ammonium binding area may be less hindered in L-SIGN than in DC-SIGN, as noted in early structural studies. This motivated us to prepare the guanidino-triazole derivative 2 (**Man84**) and study its interaction with both lectins. Here we report that **Man84** (2) is the first L-SIGN selective ligand. It binds to L-SIGN with μM affinity and has a surprising 50-fold selectivity for L-SIGN over DC-SIGN. The structure of the L-SIGN/**Man84** complex was obtained by X-ray crystallography and helped to explain the source of this selectivity. NMR studies allowed us to examine the binding process in solution for both lectins, confirming the binding selectivity and highlighting the structural differences between the two complexes. Dimeric constructs bearing two copies of **Man84** were also prepared. This low level of multivalency allowed nM affinity to be reached for L-SIGN and increased the selectivity up to 3 orders of magnitude against DC-SIGN. Finally, the ability of the divalent constructs to block DC-/L-SIGN mediated infection of host cells by Ebola and SARS-CoV-2 viruses was investigated, revealing that they are powerful inhibitors of the process.

Results and discussion

Synthesis

Synthesis of Man84. The monovalent ligands examined in this study are shown in Fig. 1. The synthesis of 1 (**Man79**) was previously described.[34]

The guanidine analogue 2 (**Man84**) was prepared by CuAAC reaction of the 2-azido-mannoside 3 (ref. 24) with alkyne 4, in
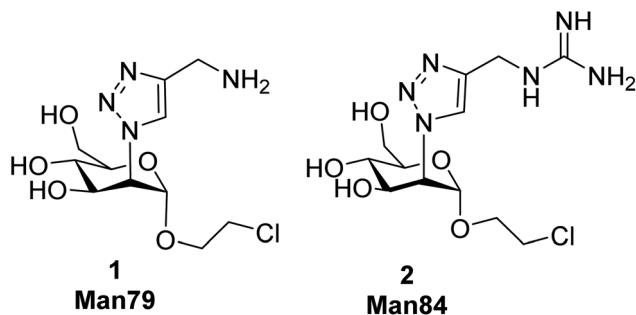
Fig. 1 Monovalent ligands analyzed in this study.

turn prepared from propargylamine **5** and Goodman reagent **6**, using a slightly adapted protocol[36,37] (Scheme 1, upper panel). The triazole product **7** was obtained with high yield (91%) and Zemplén deacetylation (0.02 M MeONa, 94%) followed by removal of the Boc protecting groups with either 20% TFA in DCM (quant) or 1 M aq. HCl in CH$_2$Cl$_2$ (3 d, 88%) afforded **2** (**Man84**) as either the TFA or chloride salt, in high purity.

Synthesis of dimers (PM69 and PM74 from Man84; PM68 and PM70 from Man79). Dimeric presentations of **Man79** (**PM68** and **PM70**) and **Man84** (**PM69** and **PM74**) were prepared using a rod-like divalent scaffold, **Rod3** (ref. 38) (Scheme 3) that we previously employed for the synthesis of multivalent DC-SIGN ligands.[39,40] We were able to show that this rod-like core has the appropriate size to bridge adjacent sites in DC-SIGN tetramers.[34,41] Since the distance between L-SIGN sugar binding sites is reportedly longer[42,43] (Fig. 9B), two PEG linkers of different lengths were adopted in the design of the dimers. The monovalent spearheads were installed using CuAAC ligation, so the azides **8** and **9** (Scheme 2) were prepared starting from **10** (ref. 34) (a precursor in the synthesis of **Man79**) via a series of functional group modifications and protecting group adjustments.

The synthesis of the dimers was adapted from the previously reported one[39] and adjusted for the solubility properties and size of the targeted ligands, which had an impact on the purification methods that were viable in this case (Scheme 3). Thus, **TIPS-Rod3** (ref. 38) was desilylated as described (TBAF, THF)
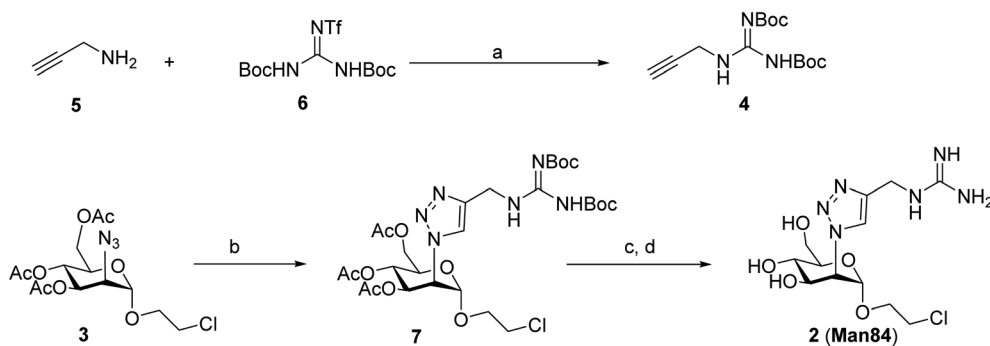
a. CH$_2$Cl$_2$, Et$_3$N, room temp, 3h, 73%; b. **4**, CuSO$_4$.5H$_2$O, Na-ascorbate, 1:1 H$_2$O:THF, room temp, 18h, 91%; c. 0.02 M MeONa, MeOH, room temp. 2h, 94%; d. 20% TFA in CH$_2$Cl$_2$ (**2** TFA salt) or 1M aq HCl in CH$_2$Cl$_2$, 3 d, 88% (**2** chloride salt)
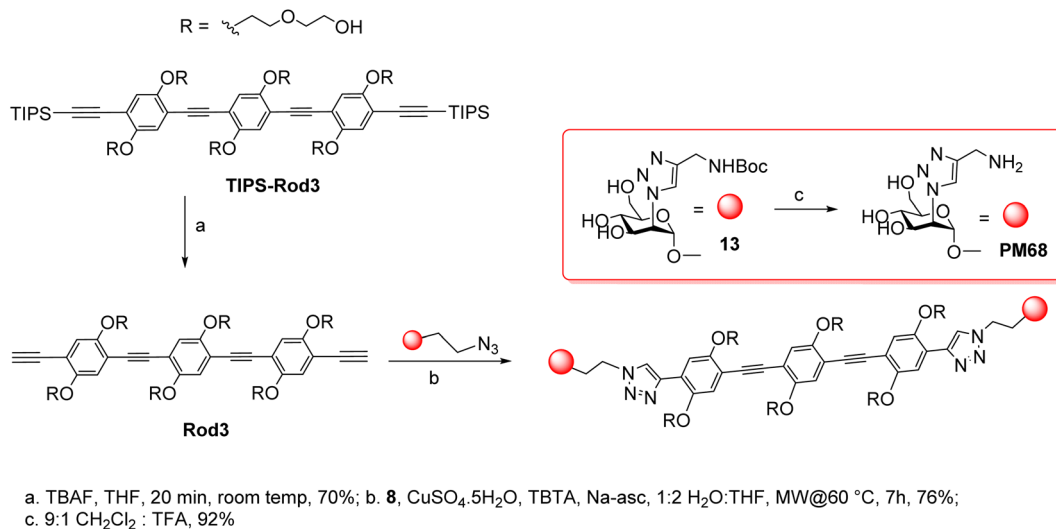
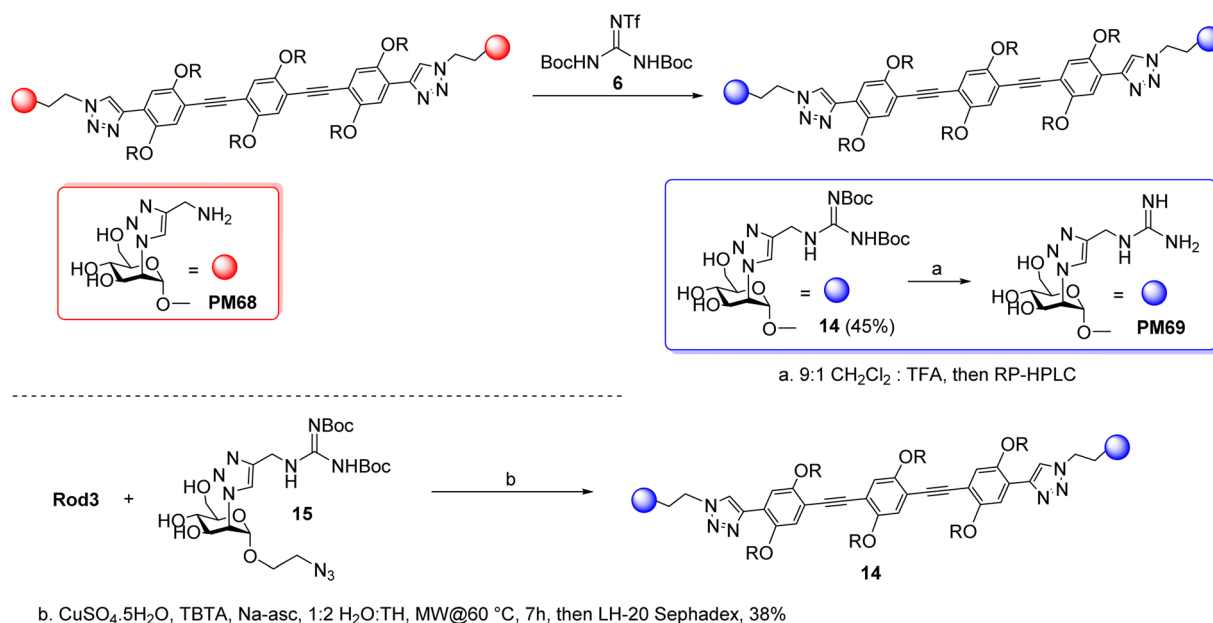**Scheme 1** Synthesis of **2** (**Man84**).
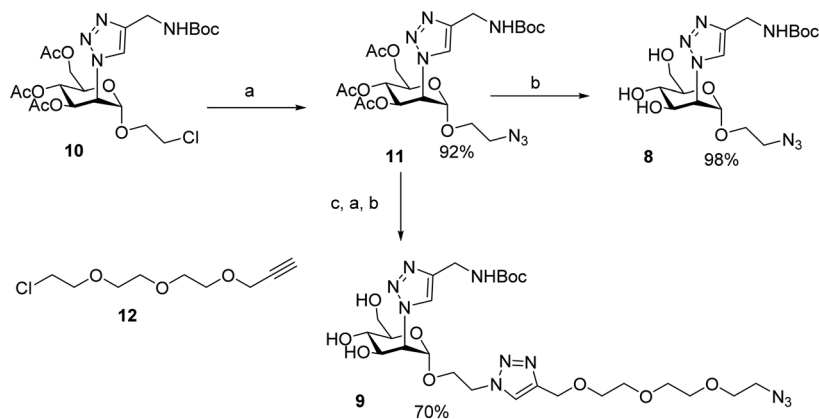
a.NaN$_3$, DMF, 55 °C, 3-5 d; b. NaOMe, MeOH, room temp., 1h; c. **12**, CuSO$_4$·5H$_2$O, Na-asc, H$_2$O: THF 1:1, RT, 16 h

Scheme 2 Synthesis of the monovalent ligands **8** and **9**.

a. TBAF, THF, 20 min, room temp, 70%; b. **8**, CuSO$_4$.5H$_2$O, TBTA, Na-asc, 1:2 H$_2$O:THF, MW@60 °C, 7h, 76%; c. 9:1 CH$_2$Cl$_2$: TFA, 92%

Scheme 3 Synthesis of **PM68**.

b. CuSO$_4$.5H$_2$O, TBTA, Na-asc, 1:2 H$_2$O:TH, MW@60 °C, 7h, then LH-20 Sephadex, 38%

Scheme 4 Synthesis of **PM69** was achieved both by direct guanidinylation of **PM68** (upper panel), or via CuAAC of **15** with **Rod 3** (lower panel), with similar results.

and the bis-alkyne **Rod-3** was chromatographically isolated to remove the tetrabutylammonium salts. CuAAC ligation of **8** was performed at 60 °C, under microwave irradiation, until complete consumption of **Rod3** was observed by TLC (9 : 1 CH$_2$Cl$_2$: MeOH). Crude **13** was purified via reverse-phase automated chromatography (76%). Boc-removal was performed at 10 mM in a 9 : 1 DCM : TFA solution, the crude was purified by RP HPLC (water/CH$_3$CN gradient with of 0.1% HCOOH) and **PM68** was isolated in 92% yield as the double formate salt.

The synthesis of the corresponding guanidine derivative **PM69** was attempted by direct guanidinylation of **PM68** by Goodman reagent **6** (CH$_2$Cl$_2$, Et$_3$N), which afforded **14** in 41% yield, after gel filtration on LH-20 Sephadex (Scheme 4, upper panel). As an alternative approach, reaction of **Rod3** with azide **15**, obtained from **8** as detailed in the ESI section,† afforded **14** in 38% yield upon gel filtration (Scheme 4, lower panel). Deprotection of the guanidine group (9 : 1 CH$_2$Cl$_2$: TFA) and isolation by RP HPLC afforded **PM69**.

With a similar approach, the long-linker dimers **PM70** and **PM74** (Fig. 2) were prepared as detailed in the ESI section.†

Surface plasmon resonance determination of the inhibitory power of Man84 and Man79 towards DC-SIGN and L-SIGN

The entire extracellular domain (ECD), a soluble form of both receptors, was used to maintain their tetramerized state for ligand evaluation. Given the size of the ligands and their
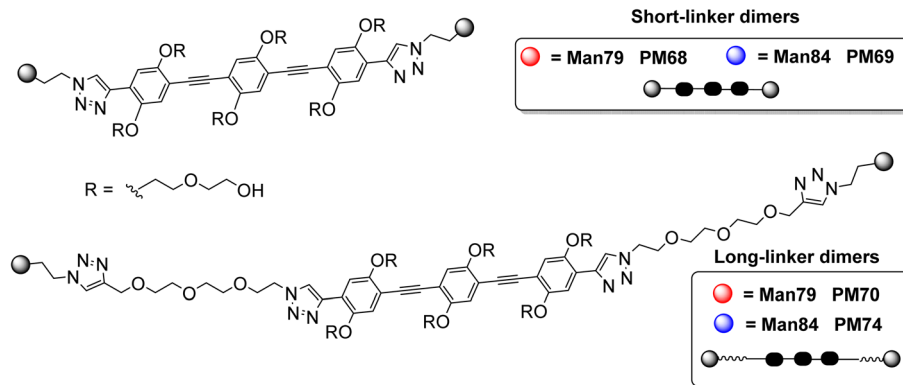
Fig. 2 The four divalent ligands analyzed in this study: **PM68** and **PM70** are a divalent presentation of the amino-substituted ligand **Man79**; **PM69** and **PM74** are divalent presentations of the guanidine-substituted ligand **Man84**. For each monovalent spearhead, a short linker and a long linker presentation were prepared.
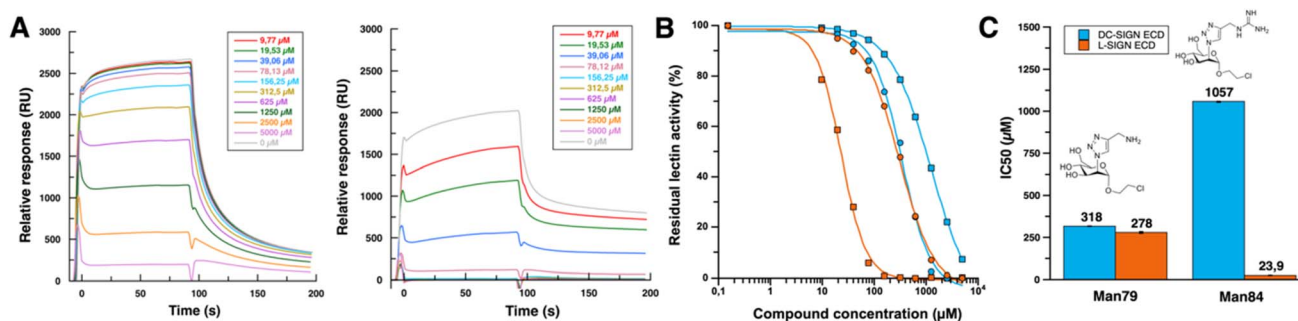

Fig. 3 (A) Sensorgrams of DC-SIGN binding inhibition (left panel) and L-SIGN binding inhibition (right panel) by **Man84**. Range of **Man84** concentrations goes from 5 mM to 10 μM by serial dilution by a factor of 2 with same color code for both DC-SIGN and L-SIGN inhibition. (B) SPR inhibition curves for **Man79** (circle) and **Man84** (square) (see ESI† for all sensorgrams). Inhibition curves concerning DC-SIGN are represented in blue and L-SIGN in orange. **Man79** data, were already described in Pollastri et al.,[34] and are shown here for direct comparison with **Man84** data. (C) IC_{50} values of **Man79** and **Man84** for DC-SIGN (in blue) and L-SIGN (in orange). Values represented are the corresponding IC_{50}.

potential low affinity for lectins, monovalent ligands were evaluated using a competition assay for binding to the SARS-CoV-2 spike protein. In this SPR assay recently described,[34] increasing concentrations of the glycomimetics were used to inhibit DC/L-SIGN binding to a surface functionalized with SARS-CoV-2 Spike glycoprotein (Fig. 3A). IC_{50} were obtained from the resulting inhibition curves (Fig. 3B and C) for both DC-SIGN and L-SIGN.

Comparison of the inhibition curves (Fig. 3B) indicates that there is no difference in the inhibitory potential of **Man79** towards either of the lectins, given the similarity of the IC_{50} values obtained towards DC-SIGN and L-SIGN (318 and 278 μM respectively). However, these values are 10 times lower than the natural mannose residue ($IC_{50} \sim 2$–3 mM), confirming that the addition of this 2-triazol-amino group at C_2 is highly efficient in raising affinity for both lectin sites, while it does not induce any selectivity, as already described.[34] This compound is a monosaccharide derivative of a previously characterized disaccharide glycomimetic where the amine has been shown to reach a specific pocket, in proximity to the calcium binding site of DC-SIGN,[24] made of the F313, E358 and S360 binding triad in DC-SIGN. These residues are strictly conserved in L-SIGN (F325,

E370 and S372) suggesting that **Man79** will bind exactly the same way in both lectins. These compounds, together with a large series of other ligands previously tested,[34] illustrate the difficulty to generate a selectivity between these two highly homologous targets.

However, one related compound seems to have achieved this feat. Sensorgrams derived from inhibition of DC-SIGN and L-SIGN by **Man84** (Fig. 3A) show a high relative response without ligand (2500 RU for DC-SIGN and 2000 RU for L-SIGN), which decreases as the glycomimetic concentration increases, reflecting an inhibitory effect on lectins activity. For the same ligand concentration, we observe a huge difference in signal between the two lectins, where the L-SIGN response is inhibited much more rapidly. Above a ligand concentration of 156 μM, the L-SIGN binding response is close to 0, compared with over 2000 RU for the same concentration to inhibit DC-SIGN interaction. The addition of a guanidium group on the triazole moiety (**Man84** compound) resulted in enhancement of inhibitory potential towards L-SIGN ($IC_{50} = 23{,}9$ μM) by a factor of 81 relative to mannose ($IC_{50} = 1.94$ mM),[34] but only by a factor of 3 towards DC-SIGN ($IC_{50} = 1.06$ mM vs. $IC_{50} = 3$ mM for mannose).[34] Thus, **Man84** exhibits a binding affinity for L-SIGN
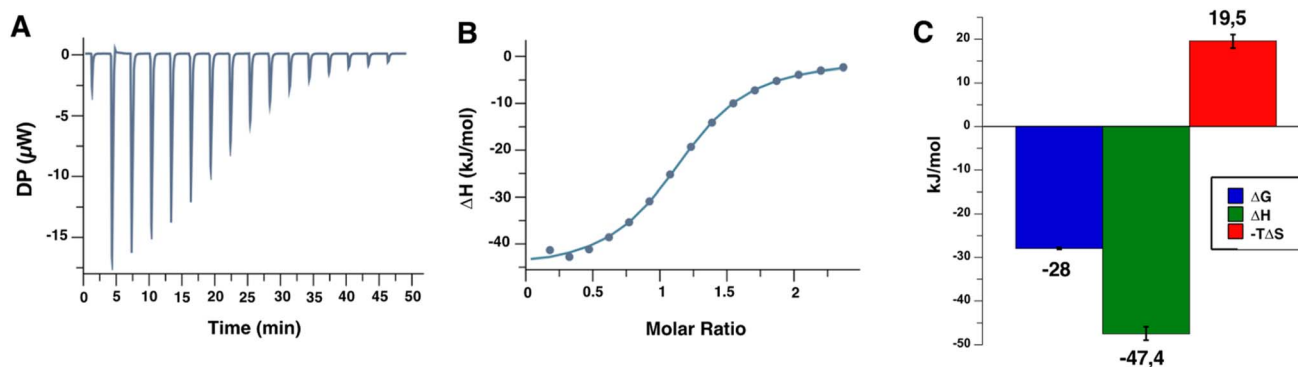
Fig. 4   Titration of the **Man84** ligand at 2 mM to L-SIGN ECD (172 μM) by ITC. (A) Representative data among a series of 3 of the titration thermograms obtained (see ESI† for all ITC titration experiments). (B) Data integration with fitted curve, using 1 : 1 binding model. (C) Average thermodynamic parameters values obtained following the L-SIGN CRD/**Man84** complex formation.
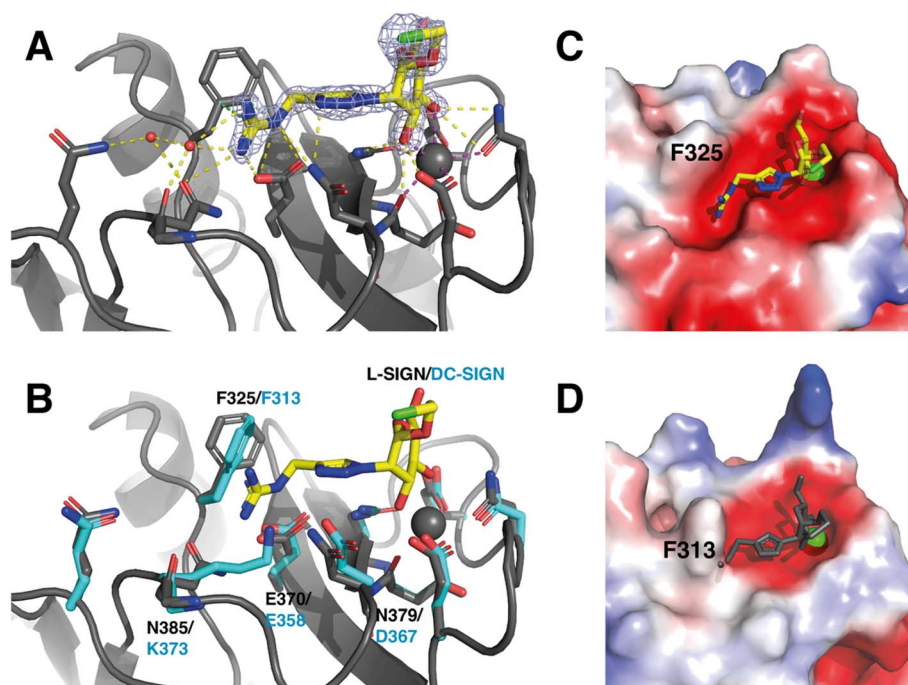

Fig. 5   3D structural binding mode of **Man84** within L-SIGN CRD and mechanism of selectivity. (A) Structure of the L-SIGN CRD/**Man84** complex (PDB: 8RCY). **Man84** is shown superimposed over the $F_o - F_c$ electron density map (light blue, 2σ contour) within L-SIGN CRD. Side chain of residues involved in the binding are represented as sticks. H-Bonds are represented as yellow dashed lines, Ca^{2+} coordination bond as magenta dashed line and π-cation interaction by green dashed lines. Water molecules are represented as red spheres. (B) Alignment with the CRD of DC-SIGN (PDB: 2IT6) for comparative purposes. Side chain of corresponding residue from DC-SIGN CRD are presented as cyan sticks and labelled. Electrostatic surfaces of L-SIGN CRD (C) and DC-SIGN CRD (D) were calculated *via* the PyMol software, with complexed **Man84** represented in yellow in L-SIGN CRD or in grey in DC-SIGN CRD where it has been added by structural alignment for comparison. The Ca^{2+} ion in the binding site is represented by a grey sphere (see Table S1† for data collection and structure refinement statistics).

that is over 40 times greater than that for DC-SIGN. The IC_{50} value in the low micromolar range firmly establishes **Man84** among the most potent monovalent glycomimetics reported so far for a C-type lectin target. Additionally, these data suggest that the guanidinium group establishes interactions with L-SIGN that cannot be formed with DC-SIGN, suggesting a distinct binding mode compared to **Man79**.

Characterization of L-SIGN/Man84 complex formation *via* isothermal titration calorimetry. Further characterization of the

lectin/ligand complex was performed by isothermal titration calorimetry of L-SIGN with **Man84** (Fig. 4).

Triplicate measurements by ITC determined an equilibrium dissociation constant K_D of 12.7 μM ± 1 μM with a 1 : 1 stoichiometry of binding. This is in full agreement with the IC_{50} evaluated above from the SPR competition experiments. It is striking to find such an increase in affinity by a factor of 230, compared to the natural mannose residue, resulting from this unique modification in C_2.[34]

The determination of the thermodynamic parameters of the L-SIGN/**Man84** complex formation reveals an average variation of enthalpy (ΔH) of -47.4 ± 1.5 kJ mol^{-1}, and a variation of entropy ($-T\Delta S$) of 19.5 ± 1.6 kJ mol^{-1}, leading to a ΔG of -28 ± 0.2 kJ mol^{-1}. It suggests an enthalpy driven complex formation as the major driving force, with a strong contribution to the interactions of the triazole-guanidium group added in position 2 within the L-SIGN active site. The observed entropy variation is likely due to loss of conformational freedom upon binding and solvent contribution.

Crystal structure of L-SIGN/Man84 complex. Co-crystallization screenings were carried out by mixing the CRD of L-SIGN with the **Man84** molecule. Crystals were obtained and their diffraction properties were tested and a data set could be

collected for a crystal of the complex. Structure of the complex was solved with 1.8 Å resolution. Results are presented in Fig. 5.

The ligand interacts in the active site of L-SIGN with its mannose moiety coordinating the Ca^{2+} ion in the canonical interaction site through its C3 and C4 hydroxyl groups (Fig. 5).[44] In addition, the guanidinium end of the ligand makes a salt bridge with Glu370 in the cleft close to the active site (Fig. 5A). This group also forms a network of electrostatic interactions and hydrogen bonds with adjacent residues in the active site such as Asn385 and Asn379, which is consistent with the thermodynamic profile obtained with the ITC assays. There is a π-cation interaction between the electronegative dipole induced by the aromatic ring of Phe325 and the positive charge of the **Man84** guanidine. As this guanidinium group is positively charged in solution, it is thus perfectly complementary to the
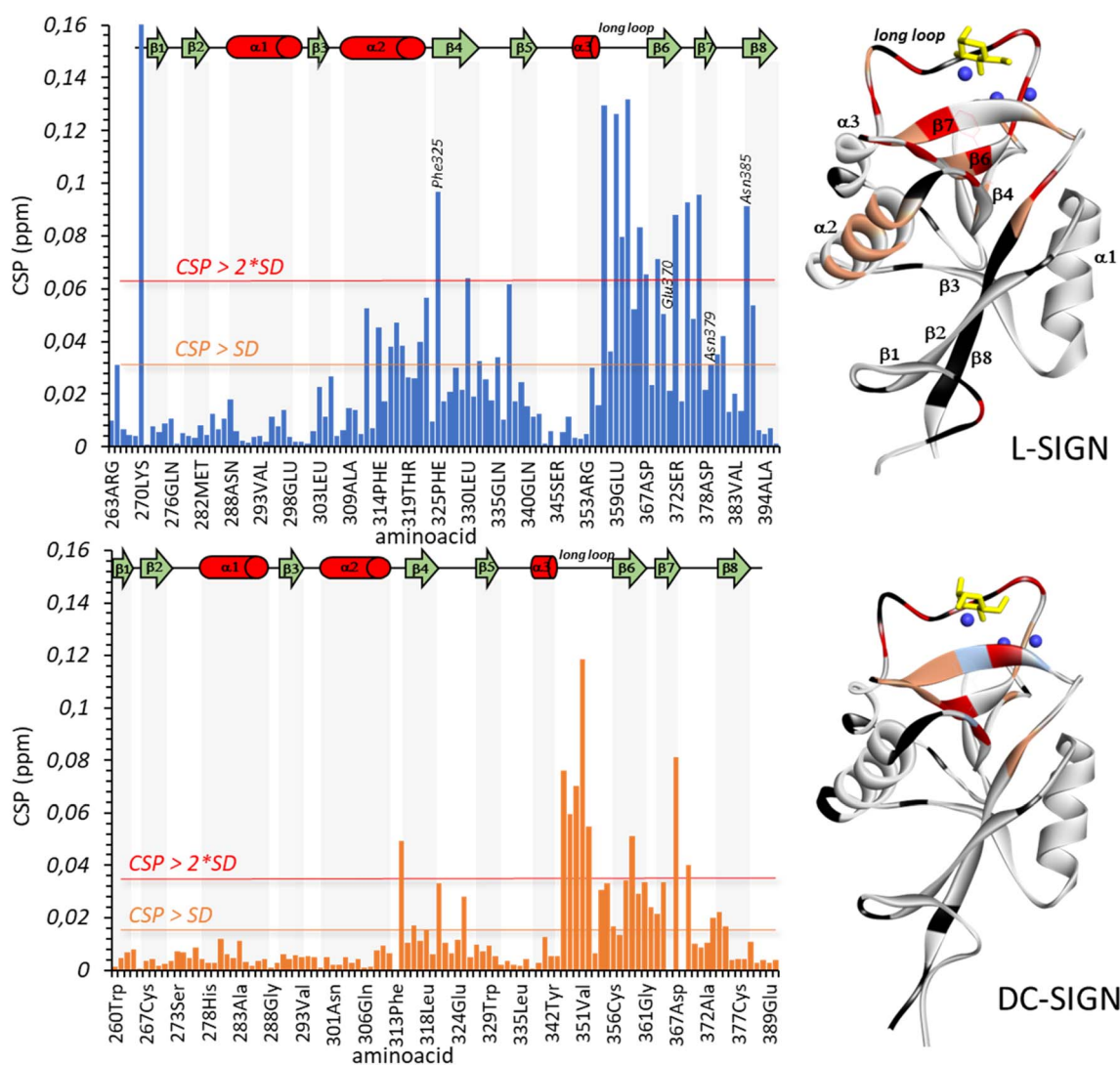

Fig. 6 The binding of **Man84** to L-SIGN (top) and DC-SIGN (bottom) in solution, by monitoring NMR signals of the corresponding protein in the absence and presence of the ligand (30 equivalents in the case of L-SIGN, and 100 equivalents for DC-SIGN). On the left, plots for the CSP analysis (average chemical shift difference between protein free and bound states) and on the right 3D cartoon representation of the corresponding protein highlighting the most affected residues in the CSP analysis: in red residues with CSP above twice the standard deviation (SD) of the whole data set, and orange residues with CSP above the SD. Residues in black are not assigned or are prolines. Residues in light blue disappear in the bound state. The ligands are in yellow and Ca^{2+} ions in dark blue. For L-SIGN, residues involved in direct intermolecular interactions with **Man84** as found by X-ray crystallography are annotated in the CSP plots.

electronegative pocket close to the calcium site and extending under Phe325 in L-SIGN (Fig. 5C). To note, the guanidinium group also contributes to the stabilization of two water molecules within the structure that contribute additional H-Bonds to the whole complex (Fig. 5A). These crystallographic water molecules, stabilized within the complex due to **Man84**, could participate to entropy contribution observed upon binding. Finally, comparison with the active site of DC-SIGN (PDB: 2IT6), revealed the atomic details that determine the selectivity of **Man84** between the lectins (Fig. 5B). It lies in differences within the guanidium-binding pocket: all the side chains interacting with **Man84** are exactly identical or equivalent in DC-SIGN and in L-SIGN except for N385, which is replaced by K373 in DC-SIGN. Thus, the electronegativity of the cleft present in L-

SIGN, critical to accommodate the guanidium group, is first cancelled by the positive side chain of K373 but also filled by this larger side chain (Fig. 5D). Thus, **Man84** cannot interact similarly with DC-SIGN, given the steric hindrance and the electrostatic repulsive effect with the guanidinium. Here a single amino acid difference between two very conserved sites, explains a 40-fold selectivity mechanism.

The binding of Man84 to L-SIGN and DC-SIGN in solution by nuclear magnetic resonance. The interaction in solution between **Man84** and L-SIGN and DC-SIGN was monitored by NMR. First, a chemical shift perturbation (CSP) analysis of the proteins upon **Man84** binding was carried out. For L-SIGN, the addition of 10 equivalents of the ligand resulted in almost complete saturation of the protein, while the addition of 100
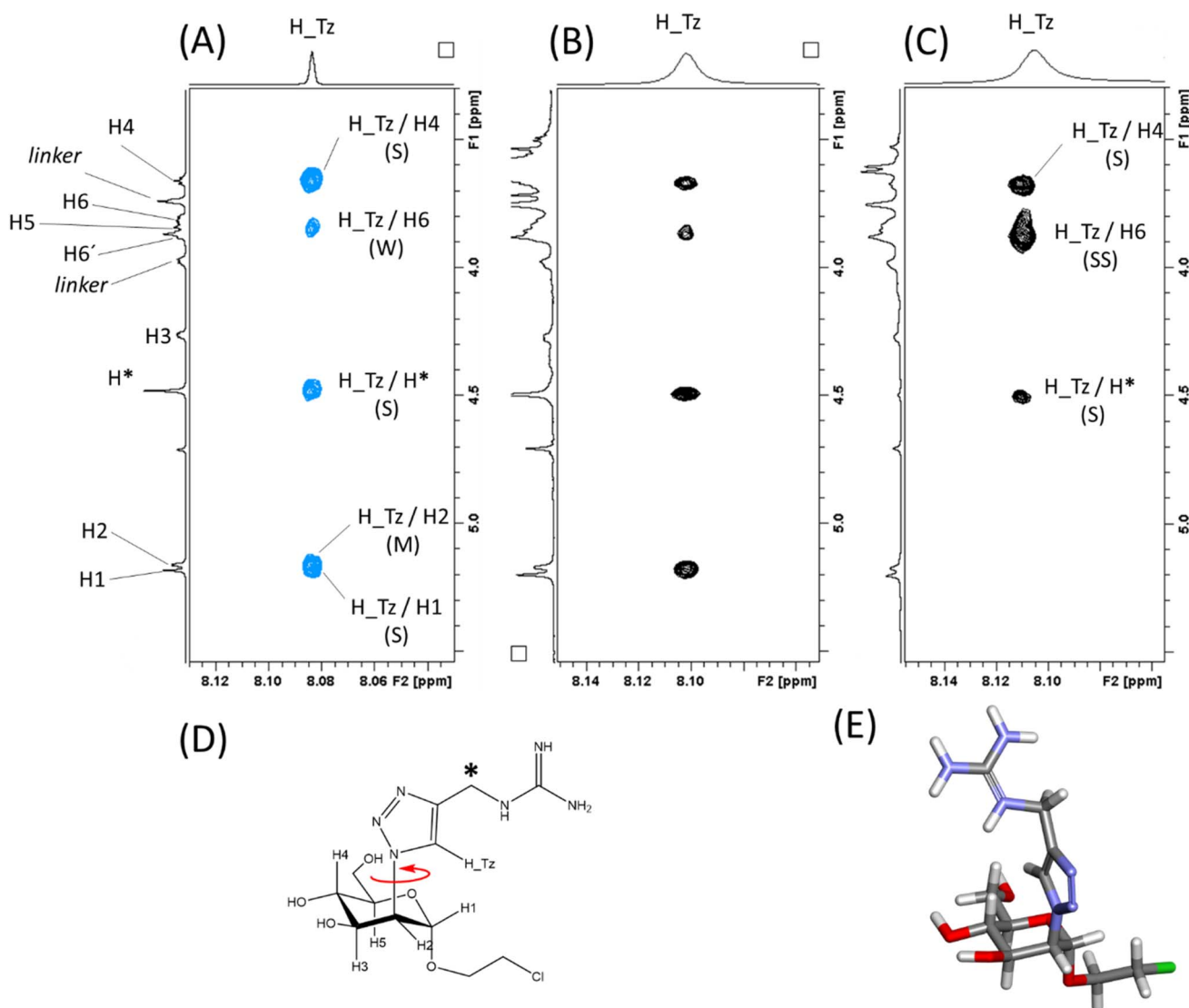

Fig. 7 The binding of **Man84** to DC-SIGN and L-SIGN in solution from the ligand perspective. Blue contours correspond to positive NOE, while black contours correspond to negative NOE. (A) NOESY spectrum of **Man84** showing the positive NOE correlations of H_Tz. (B) The same region of the trNOESY spectrum of **Man84** in the presence of DC-SIGN (1 : 17 protein : ligand molar ratio). (C) The same region of the trNOESY spectrum of **Man84** in the presence of L-SIGN (1 : 10 protein : ligand molar ratio). (D) Structure of **Man84** showing the free rotation around the C2(Man)–N(Triazol) bond. (E) The L-SIGN-bound conformation of **Man84**, as derived by NMR interaction data. This conformation corresponds to the one observed in the X-ray structure (Fig. 5A).

equivalents to DC-SIGN did not achieve saturation, highlighting the important difference in affinity for the two systems. Fig. 6 shows the CSP plot for the binding of L-SIGN (top) and DC-SIGN (below) to **Man84**. The differences are evident. While residues located at the long loops surrounding the Ca^{2+} binding site are similarly perturbed in both lectins, some remote regions are exclusively perturbed in the case of L-SIGN. That is the case of the α2 helix and the beginning of β8-strand, which flanks residue Phe325, one of the most affected residues in L-SIGN. Curiously, the most perturbed residue was Lys270, at the N-terminus and far away from the protein binding site, an effect previously observed for the interaction with mannose based ligands.[45] Additionally, residues at the β6 and β7 strands are more affected in L-SIGN than in DC-SIGN. These results confirm that **Man84** binds to DC-SIGN and L-SIGN in a different manner. While the same CSP profile is observed for **Man84** and for a single mannose residue (data not shown), where basically only amino acids at the primary Ca^{2+} binding site are perturbed upon binding, the experimental data obtained for L-SIGN unequivocally unravels the existence of further contacts between the protein and the studied glycomimetic.

To obtain information of the recognition process from the ligand perspective, trNOESY experiments were performed. First, a NOESY spectrum of the ligand alone was acquired, which showed positive NOEs. The most interesting piece of information in this case are the NOEs of the proton of the triazole ring (H_Tz), which define its orientation with respect to the pyranose (Man) ring (Fig. 7A). H_Tz showed strong (S) NOEs with H4Man and H1Man, and medium (M) with H2Man and H6Man. Since H4Man and H1Man/H2Man are on different sides of the sugar ring relative to the C2(Man)–N(Triazol) bond, this set of NOEs

indicates a high degree of conformational averaging around this bond (Fig. 7D).

The same experiment acquired under the same conditions but in the presence of DC-SIGN (1 : 17 protein : ligand molar ratio), showed the same set of NOEs with the same relative intensity, but with a different sign, changing for positive (fast tumbling small molecule) to negative (Fig. 6B), as expected for a DC-SIGN-bound ligand. This change in the sign indicates that the observed signals are indeed exchange-transferred NOE (trNOE) cross peaks.[46] The fact that the NOE pattern is exactly the same as in the free form (Fig. 6A and B) reveals that **Man84** bound to DC-SIGN conserves the same conformational behavior around the C2(Man)–N(Triazol) as in the free form. The same experiment performed in the presence of L-SIGN (1 : 10 protein : ligand molar ratio) (Fig. 7C) showed again negative NOE correlations (and thus trNOE), but the experimental observations were dramatically different from the previous ones. Now, the H_Tz/H1 and H_Tz/H2 correlations are lost, while those for H_Tz/H4 and H_Tz/H6 are strong and very strong, respectively. This cross-peak pattern reveals a conformational selection process upon binding to L-SIGN. The experimental data show that **Man84** is bound to L-SIGN in a particular, well-defined conformation, shown in Fig. 7E, in which H_Tz points towards H6Man and H4Man and corresponding to the one observed in the X-ray structure (Fig. 5A). These NMR data, therefore, are in full agreement with the X-ray crystallographic structure of the **Man84**/L-SIGN complex, and strongly support the rationale for the L-SIGN *versus* DC-SIGN selectivity. For DC-SIGN, the aglycon in **Man84** keeps the same conformational flexibility as in the free state, corroborating that this moiety is not involved in direct and persistent
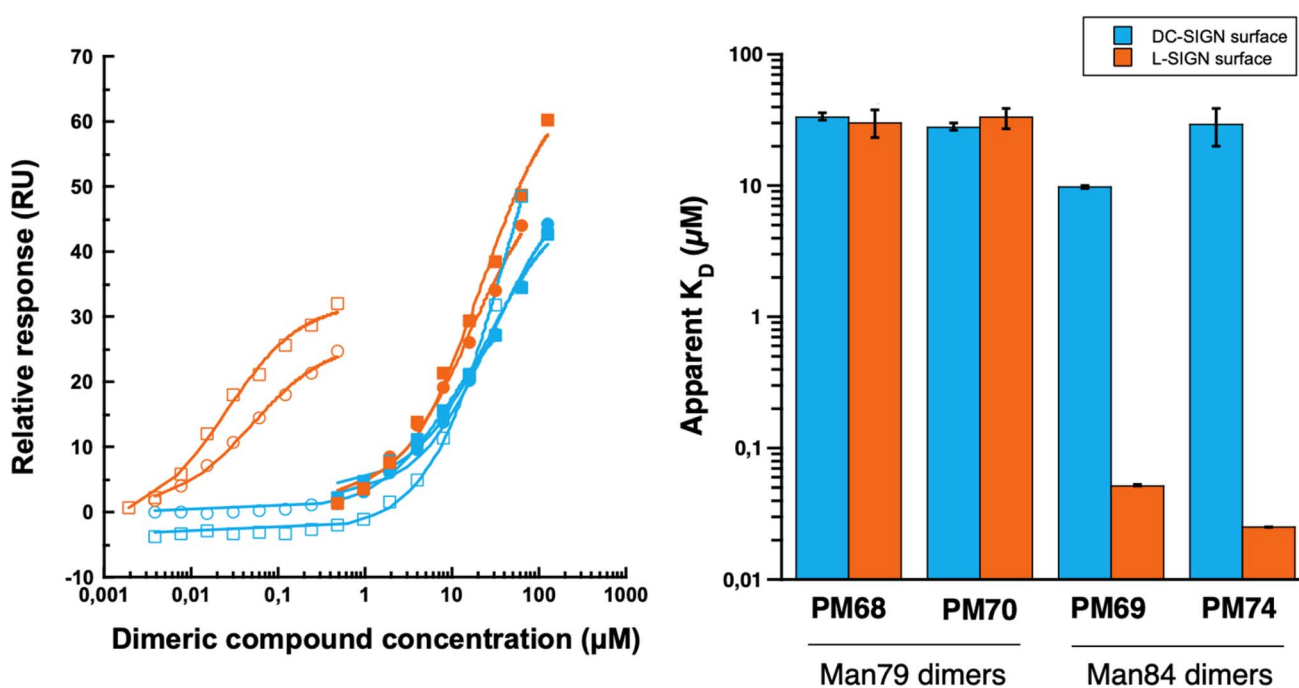

Fig. 8 SPR interaction tests with titration of **PM68** (filled circles), **PM69** (empty circles), **PM70** (filled squares) and **PM74** (empty squares) on DC-SIGN ECD (blue curves) and L–SIGN ECD (orange curves) oriented surfaces. Range of interactions were performed in duplicates.

intermolecular interactions with the lectin. In contrast, a single conformation is selected upon binding to L-SIGN, which is in agreement with the X-ray crystallography data. There are additional contacts with the protein that strengthens the interaction from the enthalpy point of view. Moreover, this conformational selection process also accounts for the observed entropy penalty upon binding.

Determination of dimer affinity and selectivity towards L-SIGN by SPR assays. The affinity of these multivalent compounds of higher molecular mass and with a high avidity was evaluated by direct interaction (SPR) using a recently developed method to generate oriented surfaces where CLRs are presented in a way mimicking the cell surface presentation of receptors.[47] The results of these interaction tests are shown in Fig. 8.

Dimerization of **Man79** and **Man84** ligands on the rod-like scaffold appears to be very efficient and significantly improves the affinity towards the lectins (Table 1). For **Man79**, which is a weak non selective binder of both CLRs (IC$_{50}$ 318 µM and 278 µM for DC-SIGN and L-SIGN, respectively, Table 1 entry 1 and Fig. 2C) the affinity increases by an order of magnitude in the dimers **PM68** (Table 1, entry 2) and **PM70** (Table 1, entry 3), for both lectins and independent of the length of the flexible linker. Similarly, the dimers of **Man84**, **PM69** and **PM74** (Table 1, entries 5 and 6) bind to DC-SIGN in the low µM range, with an increase by up to 2 orders of magnitude relative to the monovalent spearhead (10 µM and 30 µM, respectively). The same two dimers display an apparent K_D of 52 nM (**PM69**) and 25 nM (**PM74**) for L-SIGN, confirming a strong effect of the dimerization on the affinity (β/n-factor[48] of 125 and 250, respectively) and achieving an impressive selectivity for L-SIGN vs. DC-SIGN, that reaches 3 orders of magnitude with the long linker dimer **PM74**. The effect of selectivity is almost 10 times lower for short linker

PM69 (192 for "short" **PM69** and 1200 for "long" **PM74**), clearly suggesting that distance matters.

Overall, these data suggest an important avidity phenomenon for these divalent compounds, and a chelating effect in the binding to the two lectins. Contrary to **PM26**, an hexavalent rod-based construct that we described as a potent DC-SIGN ligand and characterized recently,[41] no cumulative avidity effect coming from statistical rebinding can be expected here, since a unique spearhead is presented at each extremity of the rod core. Rather, in the present case, there is probably an optimization of chelation properties with an improved access to two adjacent CRDs within the L-SIGN tetramer. However, potential clustering effect between two adjacent tetramers on the SPR chip cannot be excluded, since a single surface density was used for this characterization in the SPR assay. The higher efficiency of the ligand with the longer linker could be explained by the topology of DC-SIGN and L-SIGN tetramers as showed in Fig. 9.

Despite the high overall homology between the two lectins (77% identity[16]), their CRDs, and thus binding sites, are not oriented in the same direction of space: while those of DC-SIGN are oriented upwards, those of L-SIGN are rather turned to the lateral side, increasing the gap between adjacent and opposite sites (between 60 and 80 Å for L-SIGN versus 40 to 60 Å for DC-SIGN). Such differential spacing and topology of the L-SIGN tetramer, with respect to DC-SIGN has been recently documented experimentally with results consistent with a larger tetramer and more outwardly exposed CRDs.[49,50] A linker that is too short may cover only a single portion of the side and not connect two sites that are facing each other, thus limiting chelation properties. Moreover, in a detailed molecular dynamic study performed recently, we have shown, for DC-SIGN multivalent binders, that distances between two internal sites

Table 1 Characterization of PM's efficiency and selectivity through calculations of β-factor and selectivity ratio. Blue entries are molecule based on **Man79** mimetic and entries in green are based on **Man84** mimetic

		DC-SIGN			L-SIGN			
		$K_{D,app}{}^a$ (µM)	IC$_{50}{}^b$ (µM)	β/n-Factor^c	$K_{D,app}{}^a$ (µM)	IC$_{50}{}^b$ (µM)	β/n-Factor^c	Selectivity^d
1	**Man79**	—	318 ± 1.2	n.a.	—	278 ± 6.9	n.a.	1.14
2	**PM68** (short)	34 ± 4.9	—	4.7^f	31 ± 14	—	4.6^f	1.103
3	**PM70** (long)	28 ± 3.6	—	5.7^f	33 ± 11	—	4.2^f	0.85
4	**Man84**	—	1057 ± 5.5	n.a.	13 ± 1^e	23.9 ± 0.2	n.a.	44
5	**PM69** (short)	10 ± 1	—	53^f	0.052 ± 2 × 10^{-3}	—	125	192
6	**PM74** (long)	30 ± 9	—	18^f	0.025 ± 1 × 10^{-4}	—	260	1200

^{a} SPR direct interaction (Fig. 8). ^{b} SPR inhibition experiments (Fig. 3C). ^{c} β factor is as defined in ref. 48 and normalized here by the valency n ($\beta/n = K_{D,monovalent}/(n \times K_{D,polyvalent})$). ^{d} $K_{D,app}$ or IC$_{50}$ ratio of DC-SIGN over L-SIGN. ^{e} As measured by ITC (Fig. 4). ^{f} K_D of the monovalent ligand not determined. β-Factor calculated using the IC$_{50}$ associated with the monovalent ligand and the $K_{D,app}$s determined for the dimeric PM compounds.
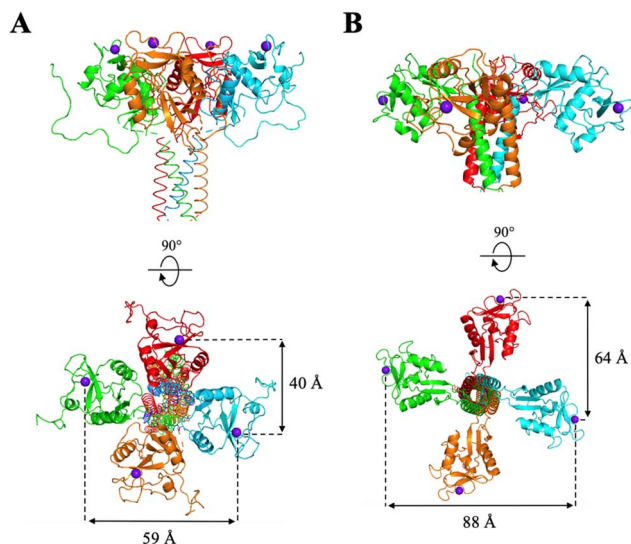
Fig. 9 Topology of DC–SIGN (panel A) and L–SIGN (panel B) active sites. Tetrameric representation issued form SAXS, X-ray crystallography studies and molecular modelling from ref. 19 and 41–43. Figures made with PyMol.

can vary, due to internal flexibility between CRDs, and that the size of the linker helps to keep chelation-binding available and buffers distance fluctuation between sites.[41] That effect might be at work here also with **PM74** *vs.* **PM69** increasing the dynamic situations where the chelation binding is still operative.

Cellular studies with EBOV and SARS-CoV-2 pseudoviruses. The efficiency of the different dimeric ligands was also

characterized in competition experiment within a cellular model of infection. First, Jurkat cell expressing either DC or L-SIGN were incubated with Ebola pseudovirus in the presence of the PM dimers (**PM68, PM69, PM70** and **PM74**) at 5 μM or 500 nM (Fig. 10). Jurkat cells were then washed and co-cultured with Vero E6 adherent cells. Cells were then lysed and assayed for luciferase expression.

The results are shown in Fig. 10 as % of trans-infection inhibition compared to the assay conducted in the absence of ligands. Mannan (Man in Fig. 10) was used as a positive control. The data indicate that all dimers at the tested concentrations are modest inhibitors of DC-SIGN mediated EBOV trans-infection (Fig. 10, left panel) and show a dose-dependent inhibition, slightly greater at 5 μM than at 500 nM. Similarly, the **Man79**-dimers **PM68** and **PM70** only partially inhibit L-SIGN mediated trans-infection of the Vero cells (Fig. 10, right panel). L-SIGN mediated trans-infection was blocked efficiently by **PM69** and **PM74** up to 99.9% at 5 μM, confirming the activity and selectivity of these ligands in a cellular model. The poor inhibition provided with **PM68** and **PM70** shows that the efficacy of **Man84** dimers is not only linked to the multivalency of the compounds but also to their affinity for L-SIGN. The long-linker **PM74** has a slight advantage, as previously observed in the SPR interaction studies, since it provides stronger inhibition at a 500 nM concentration than **PM69** (94% *vs.* 84%).

The same series of competitive experiments were carried out to study the inhibition of the trans-infection phenomenon with SARS-CoV-2 (Fig. 11). The inhibition of DC-SIGN mediated trans-infection is even lower than in the EBOV experiments for
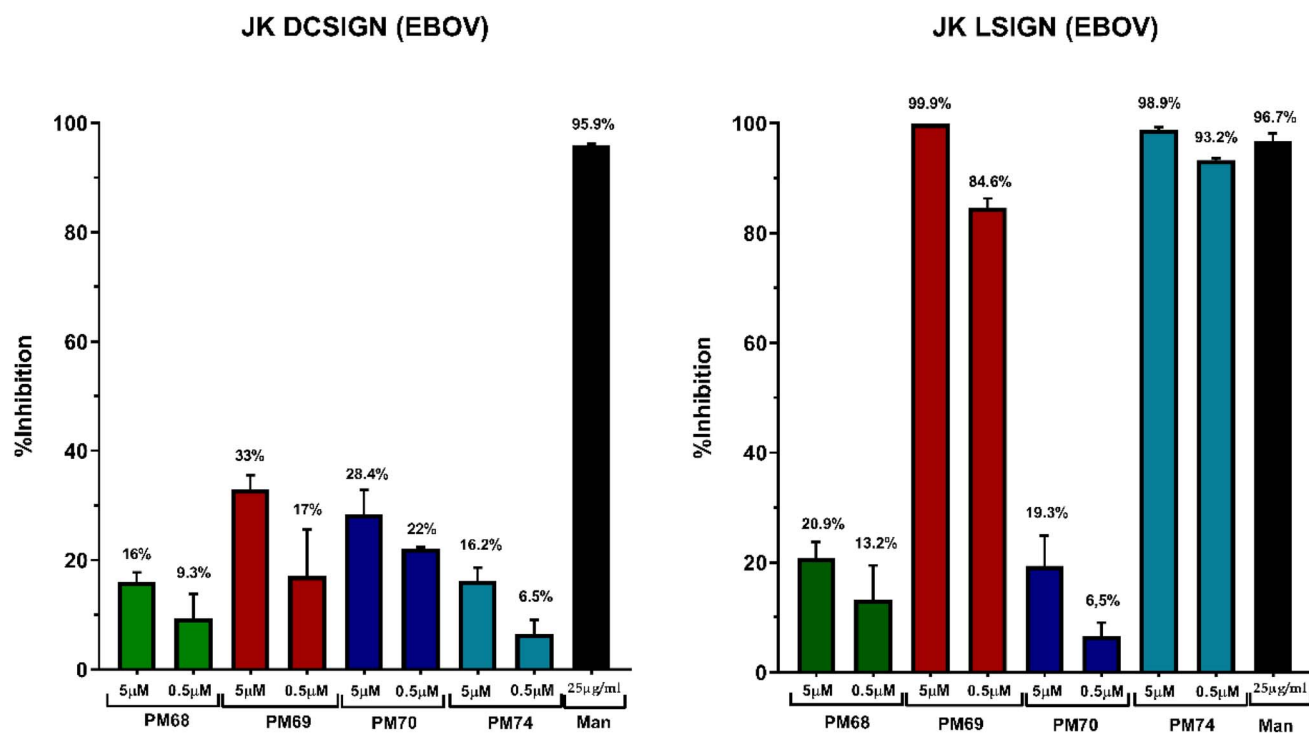

Fig. 10 Trans-infection assays of EBOV pseudotyped rVSV-luc in VeroE6 mediated by Jurkat DC–SIGN (left panel) and Jurkat L–SIGN (right panel). Results are presented as percentage of EBOV trans-infection control in the presence of compounds: **PM** ligands and mannan (Man) as compared to trans-infection of EBOV in the absence of inhibitors. The results were analyzed using GraphPad Prism v8.
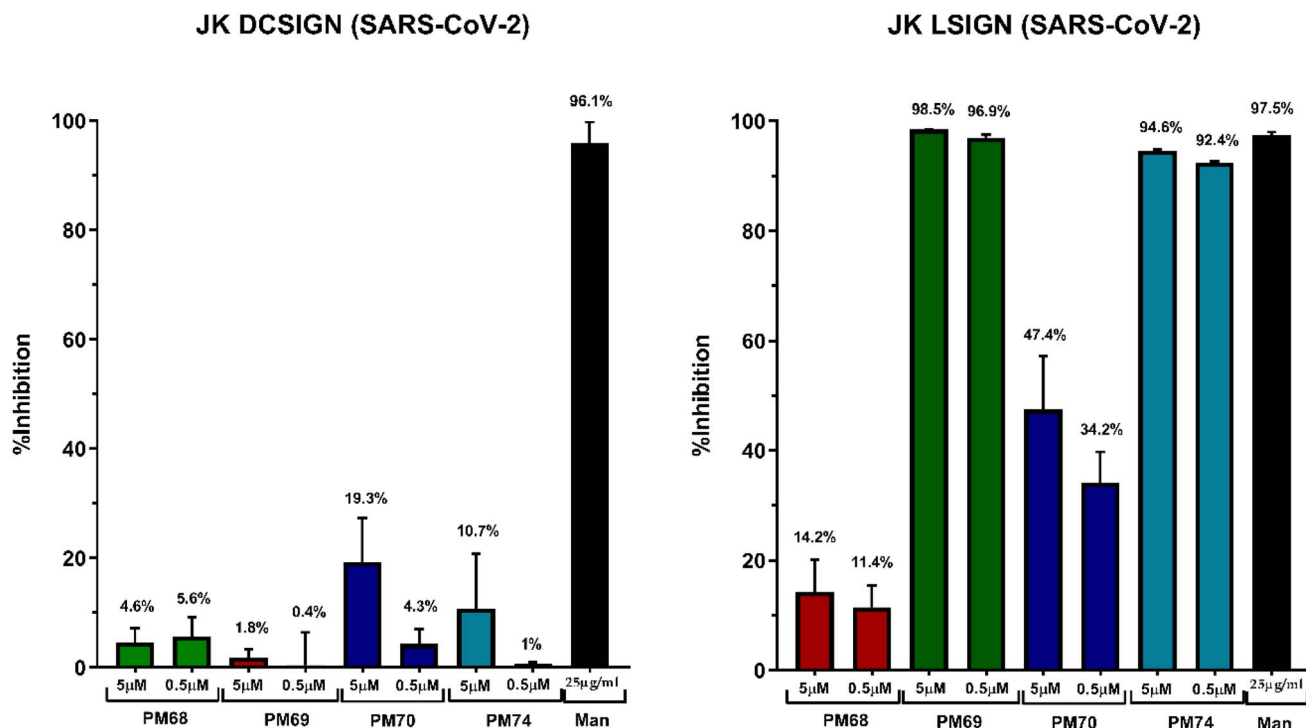
Fig. 11 Trans-infection assays of SARS-CoV-2 pseudotyped rVSV-luc in VeroE6 mediated by Jurkat DC-SIGN (left panel) and Jurkat L-SIGN (right panel). Results are presented as percentage of EBOV trans-infection control in the presence of compounds: PMs and mannan (Man) as compared to trans-infection of EBOV in the absence of inhibitors. The results were analyzed using GraphPad Prism v8.

all ligands at both the tested concentrations (here between 1% and 19% inhibition *vs.* 7% to 33% for EBOV), which is not the case for L-SIGN, further emphasizing the selectivity of **Man084**-derived PMs (**PM69** and **PM74**).

The dose-dependent effect is less pronounced for this panel of experiments: while **PM69** and **PM74** respectively inhibit infection by 98.5 and 94.6% at 5 μM, they still achieve an inhibition of 97 and 92% for a 10-fold lower dose, showing the tool's efficacy. In addition, for the SARS-CoV-2 experiments, we did not observe any differences in selectivity, whether the linker is short or long. However, given the topology of the active sites (Fig. 9), this factor should not be ruled out for future uses of these compounds. Assuming **PM74** as the most promising compound, on the basis of its molecular properties (Table 1), a wider range of concentrations of **PM74** were used in trans-infection assays with SARS-CoV-2 to derive its IC_{50}. Thus, while **PM74** IC_{50} is estimated to be >100 μM for trans-infection of SARS-CoV-2 mediated by Jurkat DC-SIGN cells, its IC_{50} is determined to be of 65 nM when using Jurkat L-SIGN cells (with 95% confidence interval 28–154 nM) (see Fig. S4†). A strong selectivity towards L-SIGN dependent SARS CoV2 trans-infection, *vs.* DC-SIGN, is demonstrated for this compound with an IC_{50} value in agreement with its $K_{D,app}$ determined on purified L-SIGN receptor (Fig. 8 and Table 1).

These inhibitions were carried out directly with the biological target of interest, the Spike protein, and therefore enabled inhibition measurements to be obtained that could be directly extrapolated to the biological interaction of interest.

Conclusion

We have described here the development of a glycomimetic ligand, **Man84**; that exclusively binds to L-SIGN with affinity in the low μM range and barely interacts with DC-SIGN. The compound selectivity has been established by several biophysical methods at the molecular and cellular level, demonstrating the viability of the tool. A structural characterization of the L-SIGN CRD/**Man84** complex allowed to determine that the origin of this selectivity lies mainly in the presence of a triazole-guanidine group, which introduces both steric and electrostatic complementarity with the L-SIGN active site, while producing unfavorable interactions in the corresponding site of DC-SIGN. To the best of our knowledge, this level of selectivity is unprecedented for glycomimetic structures targeting CLRs with similar specificity and is particularly striking because the CRDs of DC-SIGN and L-SIGN share 72% of their primary structure. On the other hand, X-ray analysis of the **Man84**/L-SIGN complex and comparison with the same region of DC-SIGN allows to locate the origin of the selectivity in a single amino acid difference (Asn385 in L-SIGN *vs.* Lys373 in DC-SIGN). This reinforces the notion that rational differential design that we have used in a different context to obtain selectivity towards DC-SIGN and against langerin[51] can be a powerful tool towards selective lectin ligands.

Through the modification at position 2 with a methylene guanidino triazole moiety, this mannose derived **Man84** showed an IC_{50} for the receptor in the micromolar scale,

gaining a 100-fold affinity compared to natural mannose ($IC_{50} \sim$ 2 mM (ref. 34)). This potential was further exploited with the dimerization of the compound on a rod-like scaffold, whose multivalency enabled to reach a nanomolar scale-affinity, most likely through chelating phenomenon. Divalency also increased the L-SIGN *vs.* DC-SIGN selectivity ratio, reaching a 1200-fold value toward L-SIGN with the most efficient ligand **PM74**.

We also showed that **PM74** can block L-SIGN mediated trans infection by SARS-CoV-2 in a cellular model. In view of the hijacking of L-SIGN by SARS-CoV-2 as a co-receptor in the respiratory tract, this tool could therefore be beneficial by competing with the anchoring of the virus. Additional applications can be foreseen for a selective L-SIGN ligand in the medical field, particularly in the prevention and treatment of viral infections and in the immunotherapy of liver tumors where L-SIGN is also abundantly expressed. In addition to this ligand, a panel of **Man84** analogues carrying guanidine isosters is currently under development. This optimization could be beneficial in order to further increase the selectivity ratio, but also to tune the basicity of the system, while maintaining the complementarity with the highly electronegative site of L-SIGN. These studies are ongoing and the results will be reported in due course.

Data availability

Crystallographic data for L-SIGN/**Man84** complex (PDB: 8RCY) has been deposited at the Protein Data Bank (PDB: https://www.rcsb.org).

Author contributions

C. Delaunay; investigation, formal analysis, visualization, writing – original draft. S. Pollastri; investigation, visualization, writing – original draft. M. Thépaut; investigation, formal analysis. G Cavazzoli, C. Bouchikri, F. Lasala, A. Franconetti; investigation. L. Belvisi; conceptualization, supervision. N. Labiod, A. Gimeno; investigation, visualization. J. Jiménez-Barbero; funding acquisition. A. Arda, R. Delgado; supervision, writing – original draft. A. Bernardi, F. Fieschi; conceptualization, funding acquisition, project administration, validation, supervision, writing – original draft, writing – review and editing.

Conflicts of interest

The authors declare the following competing financial interest(s): S. P., C. D., M. T., F. F., and A. B. declare the filing of a patent covering the use of glycomimetic L-SIGN ligands as antagonist, anti-viral adhesion, and for targeting human L-SIGN-expressing cells.

Acknowledgements

References

1 O. Takeuchi and S. Akira, *Cell*, 2010, **140**, 805–820.

2 T. B. H. Geijtenbeek and S. I. Gringhuis, *Nat. Rev. Immunol.*, 2009, **9**, 465–479.

3 S. J. Van Vliet, J. D. Dunnen, S. I. Gringhuis, T. B. Geijtenbeek and Y. Van Kooyk, *Curr. Opin. Immunol.*, 2007, **19**, 435–440.

4 G. A. Kinberger, T. P. Prakash, J. Yu, G. Vasquez, A. Low, A. Chappell, K. Schmidt, H. M. Murray, H. Gaus, E. E. Swayze and P. P. Seth, *Bioorg. Med. Chem. Lett.*, 2016, **26**, 3690–3693.

5 D. R. Dorscheid, A. E. Conforti, K. J. Hamann, K. F. Rabe and S. R. White, *Histochem. J.*, 1999, **31**, 145–151.

6 L. Dini, F. Autuori, A. Lentini, S. Oliverio and M. Piacentini, *FEBS Lett.*, 1992, **296**, 174–178.

7 J.-G. Geng, M. Chen and K.-C. Chou, *Curr. Med. Chem.*, 2004, **11**, 2153–2160.

8 T. B. H. Geijtenbeek, D. S. Kwon, R. Torensma, S. J. Van Vliet, G. C. F. Van Duijnhoven, J. Middel, I. L. M. H. A. Cornelissen, H. S. L. M. Nottet, V. N. KewalRamani, D. R. Littman, C. G. Figdor and Y. Van Kooyk, *Cell*, 2000, **100**, 587–597.

9 C. P. Alvarez, F. Lasala, J. Carrillo, O. Muñiz, A. L. Corbí and R. Delgado, *J. Virol.*, 2002, **76**, 6841–6844.

10 H. Hofmann and S. Pöhlmann, *Trends Microbiol.*, 2004, **12**, 466–472.

11 T. Gramberg, H. Hofmann, P. Möller, P. F. Lalor, A. Marzi, M. Geier, M. Krumbiegel, T. Winkler, F. Kirchhoff, D. H. Adams, S. Becker, J. Münch and S. Pöhlmann, *Virology*, 2005, **340**, 224–236.

12 M. Thépaut, J. Luczkowiak, C. Vivès, N. Labiod, I. Bally, F. Lasala, Y. Grimoire, D. Fenel, S. Sattin, N. Thielens, G. Schoehn, A. Bernardi, R. Delgado and F. Fieschi, *PLoS Pathog.*, 2021, **17**, e1009576.

13 R. Amraei, W. Yin, M. A. Napoleon, E. L. Suder, J. Berrigan, Q. Zhao, J. Olejnik, K. B. Chandler, C. Xia, J. Feldman, B. M. Hauser, T. M. Caradonna, A. G. Schmidt, S. Gummuluru, E. Mühlberger, V. Chitalia, C. E. Costello and N. Rahimi, *ACS Cent. Sci.*, 2021, **7**, 1156–1165.

14 F. A. Lempp, L. B. Soriaga, M. Montiel-Ruiz, F. Benigni, J. Noack, Y.-J. Park, S. Bianchi, A. C. Walls, J. E. Bowen, J. Zhou, H. Kaiser, A. Joshi, M. Agostini, M. Meury, E. Dellota, S. Jaconi, E. Cameroni, J. Martinez-Picado, J. Vergara-Alert, N. Izquierdo-Useros, H. W. Virgin, A. Lanzavecchia, D. Veesler, L. A. Purcell, A. Telenti and D. Corti, *Nature*, 2021, **598**, 342–347.

15 Y. Kondo, J. L. Larabee, L. Gao, H. Shi, B. Shao, C. M. Hoover, J. M. McDaniel, Y.-C. Ho, R. Silasi-Mansat, S. A. Archer-Hartmann, P. Azadi, R. S. Srinivasan, A. R. Rezaie, A. Borczuk, J. C. Laurence, F. Lupu, J. Ahamed, R. P. McEver, J. F. Papin, Z. Yu and L. Xia, *JCI Insight*, 2021, **6**, e148999.

16 E. J. Soilleux, R. Barten and J. Trowsdale, *J. Immunol.*, 2000, **165**, 2937–2942.

17 Y. Guo, H. Feinberg, E. Conroy, D. A. Mitchell, R. Alvarez, O. Blixt, M. E. Taylor, W. I. Weis and K. Drickamer, *Nat. Struct. Mol. Biol.*, 2004, **11**, 591–598.

18 Y. Guo, I. Nehlmeier, E. Poole, C. Sakonsinsiri, N. Hondow, A. Brown, Q. Li, S. Li, J. Whitworth, Z. Li, A. Yu, R. Brydson, W. B. Turnbull, S. Pöhlmann and D. Zhou, *J. Am. Chem. Soc.*, 2017, **139**, 11833–11844.

19 G. Tabarani, M. Thépaut, D. Stroebel, C. Ebel, C. Vivès, P. Vachette, D. Durand and F. Fieschi, *J. Biol. Chem.*, 2009, **284**, 21229–21240.

20 U. Svajger, M. Anderluh, M. Jeras and N. Obermajer, *Cell. Signalling*, 2010, **22**, 1397–1405.

21 V. S. F. Chan, K. Y. K. Chan, Y. Chen, L. L. M. Poon, A. N. Y. Cheung, B. Zheng, K.-H. Chan, W. Mak, H. Y. S. Ngan, X. Xu, G. Screaton, P. K. H. Tam, J. M. Austyn, L.-C. Chan, S.-P. Yip, M. Peiris, U.-S. Khoo and C.-L. S. Lin, *Nat. Genet.*, 2006, **38**, 38–46.

22 Q. Lu, J. Liu, S. Zhao, M. F. Gomez Castro, M. Laurent-Rolle, J. Dong, X. Ran, P. Damani-Yokota, H. Tang, T. Karakousi, J. Son, M. E. Kaczmarek, Z. Zhang, S. T. Yeung, B. T. McCune, R. E. Chen, F. Tang, X. Ren, X. Chen, J. C. C. Hsu, M. Teplova, B. Huang, H. Deng, Z. Long, T. Mudianto, S. Jin, P. Lin, J. Du, R. Zang, T. T. Su, A. Herrera, M. Zhou, R. Yan, J. Cui, J. Zhu, Q. Zhou, T. Wang, J. Ma, S. B. Koralov, Z. Zhang, I. Aifantis, L. N. Segal, M. S. Diamond, K. M. Khanna, K. A. Stapleford, P. Cresswell, Y. Liu, S. Ding, Q. Xie and J. Wang, *Immunity*, 2021, S1074761321002120.

23 N. Varga, I. Sutkeviciute, C. Guzzi, J. McGeagh, I. Petit-Haertlein, S. Gugliotta, J. Weiser, J. Angulo, F. Fieschi and A. Bernardi, *Chem.–Eur. J.*, 2013, **19**, 4786–4797.

24 L. Medve, S. Achilli, J. Guzman-Caldentey, M. Thépaut, L. Senaldi, A. Le Roy, S. Sattin, C. Ebel, C. Vivès, S. Martin-Santamaria, A. Bernardi and F. Fieschi, *Chem.–Eur. J.*, 2019, **25**, 14659–14668.

25 S. Sattin, A. Daghetti, M. Thépaut, A. Berzi, M. Sánchez-Navarro, G. Tabarani, J. Rojo, F. Fieschi and A. Bernardi, *ACS Chem. Biol.*, 2010, **5**, 301–312.

26 I. Sutkeviciute, M. Thépaut, S. Sattin, A. Berzi, J. McGeagh, S. Grudinin, J. Weiser, A. Le Roy, J. J. Reina, J. Rojo, M. Clerici, A. Bernardi, C. Ebel and F. Fieschi, *ACS Chem. Biol.*, 2014, **9**, 1377–1385.

27 M. Andreini, D. Doknic, I. Sutkeviciute, J. J. Reina, J. Duan, E. Chabrol, M. Thépaut, E. Moroni, F. Doro, L. Belvisi, J. Weiser, J. Rojo, F. Fieschi and A. Bernardi, *Org. Biomol. Chem.*, 2011, **9**, 5778–5786.

28 J. Cramer, *RSC Med. Chem.*, 2021, **12**, 1985–2000.

29 D. D. Nemli, X. Jiang, R. P. Jakob, L. M. Gloder, O. Schwardt, S. Rabbani, T. Maier, B. Ernst and J. Cramer, *J. Med. Chem.*, 2024, **67**, 13813–13828.

30 S. Leusmann, P. Ménová, E. Shanin, A. Titz and C. Rademacher, *Chem. Soc. Rev.*, 2023, **52**, 3663–3740.

31 V. C. Damalanka, A. R. Maddirala and J. W. Janetka, *Expert Opin. Drug Discovery*, 2021, **16**, 513–536.

32 A. Tamburrini, C. Colombo and A. Bernardi, *Med. Res. Rev.*, 2020, **40**, 495–531.

33 C. W. Davis, H.-Y. Nguyen, S. L. Hanna, M. D. Sánchez, R. W. Doms and T. C. Pierson, *J. Virol.*, 2006, **80**, 1290–1301.

34 S. Pollastri, C. Delaunay, M. Thépaut, F. Fieschi and A. Bernardi, *Chem. Commun.*, 2022, **58**, 5136–5139.

35 U.-S. Khoo, K. Y. K. Chan, V. S. F. Chan and C. L. S. Lin, *J. Mol. Med.*, 2008, **86**, 861–874.

36 K. Feichtinger, C. Zapf, H. L. Sings and M. Goodman, *J. Org. Chem.*, 1998, **63**, 3804–3805.

37 K. Feichtinger, H. L. Sings, T. J. Baker, K. Matthews and M. Goodman, *J. Org. Chem.*, 1998, **63**, 8432–8439.

38 F. Pertici, N. Varga, A. Van Duijn, M. Rey-Carrizo, A. Bernardi and R. J. Pieters, *Beilstein J. Org. Chem.*, 2013, **9**, 215–222.

39 S. Ordanini, N. Varga, V. Porkolab, M. Thépaut, L. Belvisi, A. Bertaglia, A. Palmioli, A. Berzi, D. Trabattoni, M. Clerici, F. Fieschi and A. Bernardi, *Chem. Commun.*, 2015, **51**, 3816–3819.

40 A. Berzi, S. Ordanini, B. Joosten, D. Trabattoni, A. Cambi, A. Bernardi and M. Clerici, *Sci. Rep.*, 2016, **6**, 35373.

41 V. Porkolab, M. Lepšík, S. Ordanini, A. St John, A. Le Roy, M. Thépaut, E. Paci, C. Ebel, A. Bernardi and F. Fieschi, *ACS Cent. Sci.*, 2023, **9**, 709–718.

42 H. Feinberg, Y. Guo, D. A. Mitchell, K. Drickamer and W. I. Weis, *J. Biol. Chem.*, 2005, **280**, 1327–1335.

43 H. Feinberg, C. K. W. Tso, M. E. Taylor, K. Drickamer and W. I. Weis, *J. Mol. Biol.*, 2009, **394**, 613–620.

44 H. Feinberg, R. Castelli, K. Drickamer, P. H. Seeberger and W. I. Weis, *J. Biol. Chem.*, 2007, **282**, 4202–4209.

45 F. Probert, S. B.-M. Whittaker, M. Crispin, D. A. Mitchell and A. M. Dixon, *J. Biol. Chem.*, 2013, **288**, 22745–22757.

46 A. Poveda and J. Jiménez-Barbero, *Chem. Soc. Rev.*, 1998, **27**, 133–144.

47 V. Porkolab, C. Pifferi, I. Sutkeviciute, S. Ordanini, M. Taouai, M. Thépaut, C. Vivès, M. Benazza, A. Bernardi, O. Renaudet and F. Fieschi, *Org. Biomol. Chem.*, 2020, **18**, 4763–4772.

48 M. Mammen, S.-K. Choi and G. M. Whitesides, *Angew Chem. Int. Ed. Engl.*, 1998, **37**, 2754–2794.

49 J. Hooper, D. Budhadev, D. L. Fernandez Ainaga, N. Hondow, D. Zhou and Y. Guo, *ACS Appl. Nano Mater.*, 2023, **6**, 4201–4213.

50 D. Budhadev, E. Poole, I. Nehlmeier, Y. Liu, J. Hooper, E. Kalverda, U. S. Akshath, N. Hondow, W. B. Turnbull, S. Pöhlmann, Y. Guo and D. Zhou, *J. Am. Chem. Soc.*, 2020, **142**, 18022–18034.

51 V. Porkolab, E. Chabrol, N. Varga, S. Ordanini, I. Sutkeviciute, M. Thépaut, M. J. García-Jiménez, E. Girard, P. M. Nieto, A. Bernardi and F. Fieschi, *ACS Chem. Biol.*, 2018, **13**, 600–608.